ACS APPLIED MATERIALS & INTERFACES

Research Article

www.acsami.org

Controlling the Sensing Properties of Silicon Nanowires via the Bonds Nearest to the Silicon Nanowire Surface

Jeffrey Mark Halpern,† Bin Wang, and Hossam Haick*

The Department of Chemical Engineering and Russell Berrie Nanotechnology Institute, Technion−Israel Institute of Technology, Haifa, 3200003, Israel

Supporting Information

ABSTRACT: Controlling the sensing properties of a silicon nanowire field effect transistor is dependent on the surface chemistry of the silicon nanowire. A standard silicon nanowire has a passive oxide layer (native oxide), which has trap states that cause sensing inaccuracies and desensitize the surface to nonpolar molecules. In this paper, we successfully modified the silicon nanowire surface with different nonoxide C3 alkyl groups, specifically, propyl ($Si-CH_2-CH_2-CH_3$), propenyl ($Si-CH=CH-CH_3$), and propynyl ($Si-C\equiv C-CH_3$) modifications. The effect of the near surface bond on the sensor sensitivity and stability was explored by comparing three C3 surface modifications. A reduction of trap-states led to greater sensor stability and accuracy. The propenyl-modified sensor was consistently the most stable and sensitive sensor, among the applied sensors. The propenyl- and propynyl-modified sensors consistently performed with the best accuracy in identifying specific analytes with similar polarity or similar molecular weights. A combination of features from different sensing surfaces led to the best rubric for specific analytes identification. These results indicate that nonoxide sensor surfaces are useful in identifying specific analytes and that a combination of sensors with different surfaces in a cross-reactive array can lead to specific analytes detection.

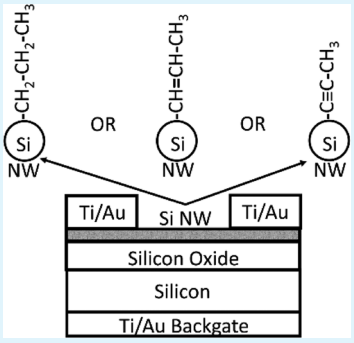

KEYWORDS: *silicon nanowire, Si−C bond, monolayer, field effect transistor, gas sensor*

INTRODUCTION

Silicon nanowire (Si NW) field effect transistors (FETs) are useful for the detection of analytes in the gas phase,[1−6] something that has been illustrated in monitoring various types of compounds.[7−9] Controllability over the sensing properties with FETs has been achieved via modification of the Si NWs surface with monolayers that have different functional terminal groups, functional chain lengths, or backbone structures.[7,8,10−16] Typically, such modifications have occurred on top of Si NW passive oxide layer,[17−20] allowing increased sensitivity and selectivity for certain analytes.[7,8,21] However, the presence of a native SiO_2 layer at the Si NW surface can screen the Si NW from the analytes to be sensed, lowering the sensitivity of the FET device.[22−25] Compared to Si NWs with native oxide, oxide-free Si NWs that have been surface-functionalized with amine-terminated alkyl monolayer via C−Si bond show dramatically improved sensitivity toward (bio)-chemical species.[26]

Recently, we showed that propenyl ($CH_3-CH=CH-$) and allyl ($CH_2=CH-CH-$) groups can give nearly full coverage of the oxide-free Si (111) surface, and the resulting Si surface provides high stability against oxidations due to $\pi-\pi$ interactions between the adjacent molecules.[18,22,27,28] Furthermore, we have shown that the density of reactive cross-linkers (for further functionalization) can be controlled without affecting the stability of the Si NWs.[18,22,28] The modification of Si NWs with $CH_2=CH-C-$ and CH_3- functionalities, which also give nearly full coverage of the Si atop sites, cannot achieve adequate stability and is therefore not appropriate for our application.[18,20,23,27,29] Also, modification of Si NWs directly with simple C_2-C_{11} alkyl chains or with backbones having benzene group(s) is not appropriate either, as they mostly cover 30−50% of the Si atop sites and exhibited a 3- to 10-fold higher oxidation rate than that of the $CH_3-CH=CH-$ Si NW.[17,18,20,22,27,28,30,31]

In the present article, we investigate the effect of the oxide removal and the effect of bond structure one bond away from the Si NW on the sensing properties of Si NW FETs when they are exposed to volatile organic compounds (VOCs) in the gas phase. The hypothesis being challenged is that different bond structures atop of the Si NW surface allow different adsorption of VOCs on the Si NW surface. Variances in the VOC surface adsorption will produce changes in the number of electrically conductive carriers between the device terminals, creating a chemical response that is distinctively different from other arrays of materials (cf. ref 32 for other systems). Therefore, understanding the bond effects on the conductivity of molecule-terminated Si NW FETs is an important component for achieving control over their sorption-induced signal, and it will be a significant focus of our research efforts.

Received: February 24, 2015
Accepted: May 11, 2015
Published: May 11, 2015

DOI: 10.1021/acsami.5b01721
ACS Appl. Mater. Interfaces 2015, 7, 11315−11321

EXPERIMENTAL METHODS

Modifications of Silicon Nanowires. Boron-doped Si NWs (p-type, ~1−8 × 10^{16} cm^{-3}) were grown on a silicon wafer (the substrate) via chemical vapor deposition (8.5 ± 1.5 μm long; 40 ± 8 nm diameter) as previously published.[33] Gold nanoparticles (~20 nm in diameter) were used as a catalyst for one-dimensional growth with SiH_4 and B_2H_6 growth gases. The gold nanoparticles, on top of the grown Si NWs, were etched away with a solution of KI/I_2 in H_2O (4:1:40 mass ratio) for 2 min. The substrate was then rinsed with ethanol and water and dried with a dry N_2 gas. The Si NWs were suspended in a buffered HF solution (6:1 40%NH_4F:49%HF) for 5 s and subsequently rinsed with water, ethanol, and isopropanol. After being dried with a dry N_2 gas, the Si NW substrate was immersed in a 90−100 °C 0.65 M PCl_5 chlorobenzene mixture with a trace of benzoyl peroxide for 10 min.[34] The substrate was rinsed with chlorobenzene and tetrahydrofuran, dried with a dry N_2 gas, and then quickly transferred into a N_2 glovebox. The substrate was immersed in a 65−80 °C alkyl magnesium salt solution, 2.0 M propylmagnesium chloride ($CH_3CH_2CH_2MgCl$), 0.5 M 1-propenylmagnesium bromide ($CH_3CHCHMgCl$), or 0.5 M 1-propynylmagnesium bromide ($CH_3CCMgCl$), in a nitrogen environment for a 15 or 24 h reaction time to achieve relatively low (~55%) or high (~100%) coverage compared to a methylated Si surface (Si−CH_3).[30] As previously reported, it is only possible to achieve ~55% coverage of the propyl groups at a 24 h reaction time.[28] To confirm surface coverage, X-ray photon spectroscopy was conducted on a wafer exposed to the alkylation process (Supporting Information, Figures S1 and S2) to confirm surface coverage.

Fabrication of the Field Effect Transistor. The alkyl-modified Si NWs were integrated into an FET device. A 40 nm titanium/110 nm gold back gate was evaporated below a highly doped silicon wafer. The modified Si NWs were unidirectionally sprayed on top of a thermally induced silicon dioxide layer (Figure 1), averaging ~50 NWs per device.[35,36] Eighteen pairs of 1300 μm long and 2 μm wide interdigitated 40 nm titanium/110 nm gold source and drain electrodes were added on top of a Si NW layer using a standard lift-off photolithography process with an AZ5214 photoresist (Karl Suss MA6). The area designated for the source drain was cleaned by oxygen plasma for 1 min and exposed to a buffered oxide etchant solution for 5 s prior to the deposition of the titanium/gold source/drain electrodes; the remainder of the wafer and the modified Si NWs were protected with the AZ5214 photoresist.[37] The photoresist was removed with *N*-methyl-2-pyrrolidone. The back gate electrodes of sensors were attached to a TO5 chip via a conductive silver paste, and the source and drain were connected through gold wire bonding.

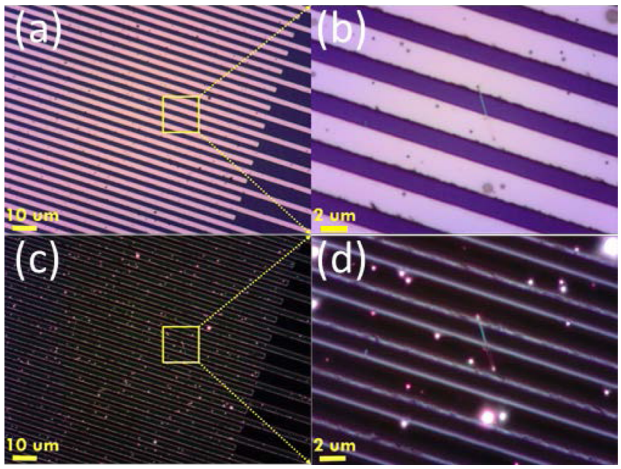

Figure 1. (left) Optical microscope (a) bright- and (c) dark-field images of the source/drain electrodes of an FET device. (right) (b) Bright- and (d) dark-field optical microscope images of zoomed electrodes region with a Si NW bridged between electrodes.

Table 1 lists the sensors used in this research. The Si NWs were modified prior to the FET device construction because the PCl_5 involved in the modification procedure can etch the Ti layer of source/drain electrodes, making the FET device fail.

Table 1. List of Surface Molecularly Modified Si NW Sensors for VOCs Detection

sensor number	molecular modification	surface coverage (%)
S1	unmodified	0
S2	propyl (Si−CH_2−CH_2−CH_3)	50 ± 10
S3	propenyl (Si−CH═CH−CH_3)	50 ± 10
S4	propenyl (Si−CH═CH−CH_3)	100 ± 10
S5	propynyl (Si−C≡C−CH_3)	50 ± 10
S6	propynyl (Si−C≡C−CH_3)	100 ± 5

Sensors Array and Gas Analyte Bubbler Systems. Sensors attached to TO5 chips were mounted onto a custom circuit board with separated sites. The sensor array was loaded into a stainless steel vacuum chamber (~170 cm^3 volume) with a vacuum output, analyte input, and air vent all controlled by pneumatic valves. The sensing measurement was performed using a Keithley 2636A SourceMeter in conjunction with a Keithley 3706 switch/multimeter. A constant drain-source voltage, V_{ds} = +2 V, was applied while sweeping the source-gate voltage V_g from +40 to −40 V. The drain-source current I_{ds}, was monitored over time. The gas analytes were created by bubbling air through a liquefied VOC at a specified flow F_a, and the remainder filled with an oil-free dry air (~8−10% relative humidity) to reach a total flow rate of F_T = 1000 mL/min. The exposure plan to the sensors for each analyte and concentration was (1) vacuum for 5 min, (2) analyte/air for 8 min, (3) vacuum for 5 min, (4) analyte/air for 8 min, and (5) vacuum for 5 min. The four concentrations used are F_a/F_T = 0.01, 0.02, 0.04, 0.08. The 12 VOCs used, hexane, octane, decane, hexanol, octanol, decanol, hexanal, cyclohexanone, ethylbenzene, toluene, methyl ethyl ketone (MEK), and chlorobenzene, were HPLC grade (Sigma-Aldrich).

Feature Extraction. The I_{ds} and V_g curve was used to determine independent features used in both the raw data evaluation and statistical analysis. The maximum I_{ds} current is defined as the on-current (I_{on}), typically at V_g = −39 V, and the minimum I_{ds} current is defined as the off-current (I_{off}), typically at V_g = 38 V. The tangent can be taken at the maximum slope of the linear region of the collected data; the intersection of that tangent with the voltage axis is defined as the V_{th}, and the slope of that tangent (dI_{ds}/dV_g) is proportional to hole mobility μ_h, as defined by eq 1. In addition, current at a specific voltage can be monitored. For example, the I_{ds} at V_g = 0 V ($I_{Vg=0}$) can be presented.

$$\mu_h = \frac{\ln[(2t_{ox} + R_{NW})/R_{NW}]}{2\pi\varepsilon_{ox}n} \frac{L_{NW}}{V_{ds}} \frac{\partial I_{ds}}{\partial V_g} \quad (1)$$

Here, the width of the gate oxide, t_{ox} = 300 nm; the radius of the Si NW, R_{NW} = 40 nm; the bridged nanowire number, n; the dielectric constant of silicon oxide, ε_{ox} = 3.45 × 10^{-11}, the length of the channel, L_{NW} = 2 μm; the constant drain-source voltage, V_{ds} = +2 V.[24] Sensing features obtained at a VOC concentration of F_a/F_T = 0.08 were used for further statistical analysis.

Linear Discriminant Analysis. Linear discriminant analysis is a supervised multivariate analysis method that uses a training set to maximize separation between supplied classifications. The statistical tool (SAS JMP, version 10 Pro) determines canonical variables (new orthogonal axes) as a linear combination of the input variables to maximize interclass variance while minimizing intraclass variance. Linear discriminant analysis uses statistics and pattern recognition to accurately identify two or more different groups of signals (or in our case analytes). If a signal is sensitive but nonreproducible, it will have poor accuracy through linear discriminant analysis. Also, only independent features are used; the square of the Pearson product moment correlation coefficient R^2 less than 0.6 is determined to be

DOI: 10.1021/acsami.5b01721
ACS Appl. Mater. Interfaces 2015, 7, 11315−11321

independent (i.e., R^2 greater than 0.6 is determined to be dependent). Through the results from linear discriminant analysis, we are able to determine which near-surface bond structures (with or without an oxide layer) have a higher sensitivity for specific analytes. Ideally, one surface will be used to accurately predict analyte type and specific analytes from the results, but results from a cross-reactive sensor array, a sensor array of different modified surfaces, will be presented for optimal analyte selectivity.

The classification accuracy is determined by a leave-one-out method. Assuming n measurements, linear discriminant analysis is computed n times using $n - 1$ data points. The left-out data point, which is not included in the training set, is projected onto the calculated model determining the classification. The accuracy is determined as the percentage of 100 × (1 − the number of misclassified points divided by the total number of data points), eq 2.

$$\%\text{accuracy} = 100 \times \left(1 - \frac{\text{leave} - \text{one} - \text{out misclassified points}}{\text{total number of data points}}\right) \quad (2)$$

RESULTS

Field-Effect Transistor Device with Modified Si Nanowires. After chemical modification via Grignard reaction, propyl-modified ($Si-CH_2-CH_2-CH_3$), propenyl-modified ($Si-CH=CH-CH_3$), and propynyl-modified ($Si-C\equiv C-CH_3$) Si NW FETs were constructed. Figure 1 displays the constructed FET device with spray-coated modified Si NWs. Typically, ~50 Si NW bridges exist on a single Si NW device.[35] The final FET devices were checked with a probe station under ambient atmosphere, and the I_{on}/I_{off} ratios were over 1×10^3—see Supporting Information, Figure S3.

Response to Analytes. The sensor surfaces were exposed to various volatile organic compounds to determine their sensitivity and selectivity to analytes. Figure 2 shows the raw data of on-current, hole mobility, and voltage threshold features displayed in a column graph with error bars at an analyte concentration of F_a/F_T = 0.08. The large error bars of the voltage threshold for sensors S1 and S2 show that these data are inaccurate and unstable, and therefore, the voltage threshold for sensors S1 and S2 will not be used in future analyses. Large error bars are not observed on the on-current or hole mobility features at any of the sensors. Also, large, reproducible variability between the VOC signals is seen in sensor S4, which indicates that a level of specificity can be achieved. In addition, the hole mobility feature was found to have relatively low standard division (SD) when surface coverage increases (from ~55% to ~100% coverage; see Supporting Information, Figure S4). The decrease in SD is expected since both sensors S4 and S6 are stable in air, and complete alkyl-coverage, with removal of oxygen (trap states) on the Si NW surface, also indicates a reduction in SD.

Using a plus/minus statistical algorithm, the sensitivity hierarchy of three sensing features (on-current, voltage threshold, and hole mobility) at F_a/F_T = 0.08 was calculated. The results were plotted in hot plots to look at sensitivity and to determine the ideal modified sensor (Figure 3). For on-current, sensors S1 and S5 were less sensitive than S2 and S3. For voltage threshold, sensor S5 was more sensitive than sensor S3. Sensors S1 and S2 were not included because of the large error bars found in Figure 2. For hole mobility, the sensors with the lowest to highest sensitivities were found to be sensors S1, S5, S3, and S2. The sensitivity hierarchy of these three sensing features at low VOC concentrations was also studied, and the same trend as the sensitivity hierarchy at F_a/F_T = 0.08 was observed (Supporting Information, Figures S5–S7).

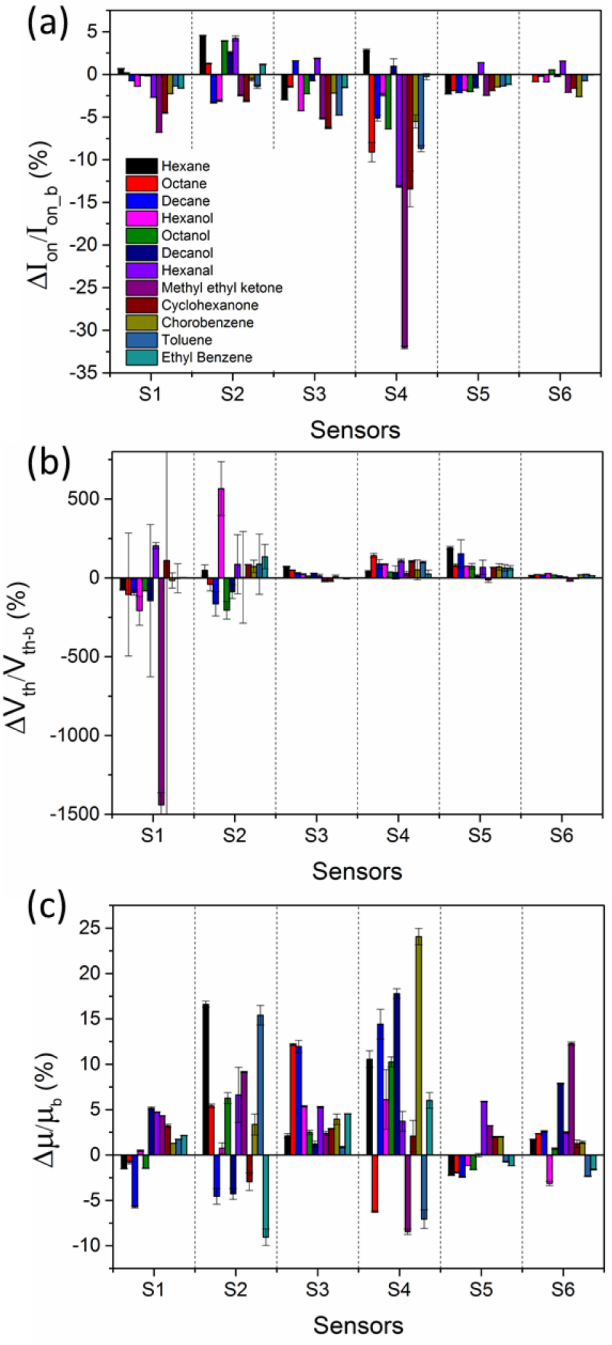

Figure 2. Column graph of (a) on-current, (b) voltage threshold, and (c) mobility of molecularly modified sensors as well as unmodified sensors at VOC concentration of F_a/F_T = 0.08. The Δ refers the sensing signal changes between VOC exposure and vacuum, and subscript "b" refers to the sensing signal in vacuum.

Performance as a Cross-Reactive Sensor Array. Each sensor has multiple independent (noncorrelated) features that can be used to determine analyte specificity. Linear discriminant analysis was used to identify analyte type and subtype signals. Separate discriminant analysis models were conducted for five groupings: (1) alcohol versus alkane; (2) alcohol versus alkane versus ketone versus aromatic rings; (3)

DOI: 10.1021/acsami.5b01721
ACS Appl. Mater. Interfaces 2015, 7, 11315−11321

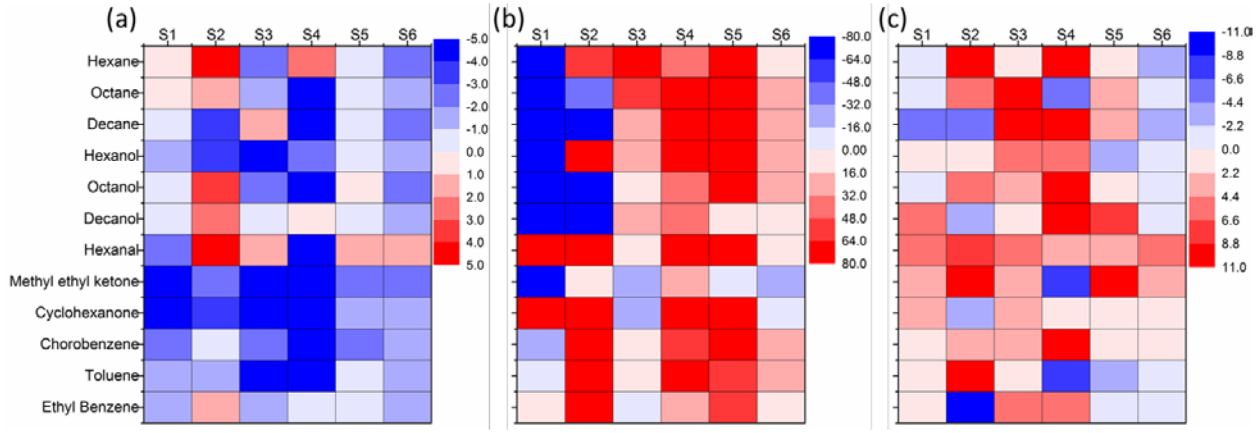

Figure 3. Hot plot (sensitivity hierarchy) in (a) on-current, (b) voltage threshold, and (c) mobility of molecularly modified sensors as well as unmodified sensors at VOC concentration of F_a/F_T = 0.08.

subtypes of alkanes (hexane vs octane vs decane); (4) C_6 molecules (hexanol vs hexane vs hexanal vs cyclohexanone); and (5) aromatic rings (toluene vs ethylbenzene vs chlorobenzene). The linear discriminant analysis model was designed to select the best noncorrelated features to optimize accuracy. The accuracy of each discriminant analysis model, with independent features selected for each sensor, is displayed in Tables 2−6.

Table 2

			sensor features		
sensor number	misclassified	accuracy[a]	1	2	3
S1	5	90%	$I_{V=-5}$	$I_{V=10}$	$I_{V=28}$
S2	11	77%	$I_{V=18}$	$I_{V=5}$	
S3	8	83%	V_{th}	I_{on}	$I_{V=28}$
S4	11	77%	I_{off}	$I_{V=18}$	V_{th}
S5	8	83%	I_{off}	$I_{V=18}$	$I_{V=-5}$
S6	6	88%	I_{off}	$I_{V=28}$	I_{on}
all sensors	1	98%	$I_{V=-5}$ (S1)	$I_{V=18}$ (S5)	$I_{V=28}$ (S6)

[a]Accuracy determined in predicting alcohol vs alkane of six different analytes using a linear discriminant analysis built around the features listed.

Linear discriminant analysis showed, first, that the sensors were capable of distinguishing between alcohols and alkanes, Table 2. Sensor S1 was the best single sensor for distinguishing between alcohols and alkanes, 90% accurate, due to its hydrophilic surface, which attracts alcohols (hydrophilic) and

Table 4

			sensor features	
modification	misclassified	accuracy[a]	1	2
S1	7	71%	$I_{V=0}$	μ_h
S2	9	63%	$I_{V=18}$	$I_{V=10}$
S3	6	75%	I_{on}	$I_{V=18}$
S4	6	75%	$I_{V=18}$	$I_{V=28}$
S5	6	75%	I_{off}	I_{on}
S6	7	71%	I_{off}	V_{th}
all sensors	5	79%	I_{off} (S5)	$I_{V=18}$ (S4)

[a]Accuracy determined in predicting alkane analyte subtypes, specifically hexane vs octane vs decane, using a linear discriminant analysis built around the features listed.

Table 5

			sensor features		
modification	misclassified	accuracy[a]	1	2	3
S1	9	72%	$I_{V=-5}$	$I_{V=5}$	$I_{V=28}$
S2	16	50%	$I_{V=18}$	$I_{V=5}$	I_{off}
S3	6	81%	I_{on}	$I_{V=18}$	$I_{V=28}$
S4	10	69%	$I_{V=18}$	μ_h	I_{on}
S5	10	69%	I_{off}	$I_{V=18}$	$I_{V=5}$
S6	7	78%	I_{on}	$I_{V=5}$	$I_{V=28}$
all sensors	5	84%	$I_{V=5}$ (S1)	I_{on} (S3)	$I_{V=18}$ (S4)

[a]Accuracy determined in predicting C_6 analyte subtypes, specifically, hexane vs hexanol vs hexanal vs cyclohexanone, using a linear discriminant analysis built around the features listed.

Table 3

			sensor features				
modification	misclassified	accuracy[a]	1	2	3	4	5
S1	14	84%	$I_{V=-5}$	$I_{V=5}$	$I_{V=28}$		
S2	29	67%	$I_{V=18}$	$I_{V=5}$	$I_{V=28}$		
S3	31	65%	$I_{V=0}$	I_{off}	$I_{V=28}$		
S4	32	64%	$I_{V=18}$	I_{on}	$I_{V=0}$	μ_h	
S5	33	63%	$I_{V=5}$	$I_{V=28}$	I_{off}	$I_{V=18}$	μ_h
S6	15	83%	$I_{V=0}$	V_{th}	μ_h	I_{off}	$I_{V=28}$
all sensors	8	91%	$I_{V=-5}$ (S1)	$I_{V=5}$ (S2)	I_{off} (S6)	I_{on} (S6)	$I_{V=18}$ (S5)

[a]Accuracy determined in predicting alcohol vs alkane vs aromatic vs ketones of 12 different analytes using a linear discriminant analysis built around the features listed.

DOI: 10.1021/acsami.5b01721
ACS Appl. Mater. Interfaces 2015, 7, 11315−11321

Table 6

			sensor features	
modification	misclassified	accuracy[a]	1	2
S1	6	75%	$I_{V=-5}$	$I_{V=10}$
S2	7	71%	V_{th}	$I_{V=10}$
S3	7	71%	I_{on}	V_{th}
S4[b]	3	88%	$I_{V=10}$	V_{th}
S5	6	75%	$I_{V=18}$	I_{on}
S6	5	79%	$I_{V=0}$	$I_{V=28}$
all sensors	2	92%	$I_{V=-5}$ (S1)	V_{th} (S4)

[a]Accuracy determined in predicting aromatic analyte subtypes, specifically, toluene vs chlorobenzene vs ethyl benzene, using a linear discriminant analysis built around the features listed. [b]The most sensitive sensor was sensor S4.

does not attract alkanes (hydrophobic) (i.e., the hydrophilic surface resulted in a relatively high signal for alcohol compared to alkanes). For this reason, sensor S1 should not be as accurate in distinguishing different types of alkanes as seen in Table 4. Sensor S2 was the least accurate, 77% accurate, due to the inconstancy in the measurement, as mentioned previously, Figure 2. Only two features were used in sensor S2 model because the other features correlate to (were not independent of) the features used. A combination of sensor features from various sensor chemistries, specifically, using the current at V_g = −5 V of sensor S1, the current at V_g = 18 V of sensor S5, and the current at V_g = 28 V of sensor S6, provided the best accuracy, 98% accurate (1/48 misclassified point).

Next, linear discriminant analysis was used to distinguish between alcohols versus alkanes versus ketones versus aromatic rings, which revealed that sensor S1 was the best, 84% accuracy, and sensor S5 was the worst, 63% accuracy, Table 3. Only three features were used at various surfaces because additional features were dependent (i.e., additional features correlate to the best features found at each sensor); more features, up to five, were accepted if the features were independent (i.e., they did not correlate). Again, because of the unmodified sensor's hydrophilic surface, the unmodified sensor exhibits high sensitivity for polar molecules (alcohol and ketones) and low sensitivity for nonpolar molecules (alkanes) leading to high accuracy in distinguishing chemicals based on "type." A combination of features and sensors was the most accurate, 91% accuracy (8/88 misclassified points), specifically, using the current at V_g = −5 V of sensor S1, the current at V_g = 5 V of sensor S2, I_{off} and I_{on} of sensor S6, and the current at V_g = 18 V of sensor S5.

Typically, distinguishing different types of alkanes, specifically, hexane versus octane versus decane, is difficult with Si NW FETs.[21] The discriminant analysis of sensor S1 found 71% accuracy, significantly reduced from distinguishing analyte types, Table 4. The most accurate sensors (75% accuracy) in determining different alkanes were sensors S3, S5, and S4. The most accurate discriminant analysis model, 79% accuracy (5/24 misclassified points), combined features from two separate sensors, specifically, using I_{off} of S5 and the current at V_g = 18 V of S4.

C_6 molecules are also difficult to distinguish using Si NW FETs because of their low molecular weight, which causes them to have a smaller effect on surface charging. Although sensor S1 was typically accurate in distinguishing molecular types (Table 2), it was inaccurate in distinguishing C_6 molecules, hexane versus hexanol versus hexanal versus cyclohexanone, with a 72% accuracy (Table 5). The most sensitive and accurate sensor in distinguishing C_6 molecules was sensor S3 (81% accuracy). A discriminant analysis model using features from three sensors, specifically, the current at V_g = 5 V of sensor S1, I_{on} of sensor S3, and the current at V_g = 18 V of sensor S4, provided the best (84%) accuracy (5/32 misclassified points). Although sensor S1 did not perform well when it was used alone, the inclusion of sensor S1 was important to achieve the higher accuracy due to the different sensing mechanism (hydrophobic/hydrophilic interaction) compared to sensor S3.

A discriminant analysis model was also used to distinguish different aromatic rings, specifically, toluene versus chlorobenzene versus ethylbenzene, Table 6. Sensor S1 was less accurate, with an accuracy of 75%, compared to sensor S4, which had an accuracy of 88%. The most accurate (92%) discriminant analysis model (2/24 misclassified points) was from combining features from two different sensors, specifically, using the current at V_g = −5 V of sensor S1 and the voltage threshold of sensor S4.

DISCUSSION

Alkyl modifications were reported on top of Si NWs via the alkyl Grignard reaction without an oxide layer.[27,28,30,34] Because of steric effects, Si NWs can only be modified with the propyl modification up to 55% coverage.[27,28] Therefore, propenyl- and propynyl-modifications were also conducted at 55% coverage for a direct comparison. Further, the Si NWs were modified at 100% coverage (meaning that every topmost Si atom has the alkyl modification, i.e., no oxide) with propenyl- and propynyl-modifications. In the 100% coverage case, no Si−O bonds were observed via XPS indicating that there was no passivated oxide layer remaining.[28] In addition, the oxygen content was monitored over time to indicate that the sensor surface remains stable over a prolonged period after being exposed to a humid environment.[28] The complete coverage has been known to have increased stability, and the complete removal of trap states is expected to increase stability and selectivity for nonpolar analytes.[28]

The effect of surface coverage on sensing characteristics was determined by comparing hot plots of sensor S3 to S4 and sensor S5 to S6. Consequentially, an increase in surface coverage induced the reduction of trap states on the surface (i.e., surface oxygen).[17] Using a plus/minus statistical algorithm, as surface coverage increased for propenyl-modified sensors, an increase in the normalized (from vacuum baseline) signal of on-current, hole mobility, and voltage threshold features was observed. As surface coverage for propynyl-modified sensors increased, an increase of the normalized signal of on-current was observed, but a sensitivity decrease of hole mobility and voltage threshold was observed (Figure 3). The increase in sensitivity from additional coverage was expected because of the reduction in trap states which produce sensing inaccuracies and reduce sensitivity.

A look at possible sensing processes with the propenyl- and propynyl-modifications would clarify why a decrease in hole mobility and voltage threshold is observed at propynyl-modified sensors. With fewer Si−OH bonds, there should be an increase in sensitivity to nonpolar VOCs specifically, because the nonpolar analytes will cause a greater charge at the Si NW surface with a reduction of trap states.[9,25] Also, the C−C bond near the Si NW surface will also affect how the response to the dielectric medium close to the surface interacts with the surrounding analytes.[9,25] The double-bond in the propenyl-

DOI: 10.1021/acsami.5b01721
ACS Appl. Mater. Interfaces 2015, 7, 11315−11321

modified sensors has the ability to transfer electrons to the adjacent C−C bond.[28] The ability to transfer electrons increases the electron cloud of the FET, thereby increasing its sensitivity. The electrons in triple bond are also delocalized; however, it has been previously reported that the propynyl modification has the ability to donate electrons to the Si NWs.[28] The reduction in sensitivity of the hole mobility and voltage threshold features occurs because of an increase in "virtual electrons" present in the Si NW. In vacuum, the raw data of sensors S5 and S6 for the hole mobility feature were 22.4 ± 0.6 $cm^2/(V{\cdot}s)$ and 43.5 ± 0.6 $cm^2/(V{\cdot}s)$, respectively. The increase of the propynyl-modified sensor features in vacuum suggests that a saturation limit was achieved with greater surface electron coverage. Overall, each surface-modified sensor has improved sensing capabilities with increased sensitivity and stability in 100% alkyl coverage, compared to 55% coverage, because of the reduction in trap states.

In summary, sensor S1 was accurate in distinguishing types of analytes, specifically, those between polar and nonpolar chemicals; however, sensor S1 was inaccurate in distinguishing between specific polar or nonpolar molecules. The increase in analyte selectivity is due to the Si−OH hydrophilic surface. However, sensors with Si−OH have a low accuracy for distinguishing nonpolar analytes. The propenyl-modified sensors performed the best at identifying specific analytes, especially nonpolar analytes. Propenyl-modified sensor surfaces, due to the $\pi-\pi$ bond, have an increased response to the dielectric medium close to the Si NW surface, which made it more sensitive to lower molecular weight analytes (C_6 compounds) and nonpolar analytes. Propynyl-modified sensor surfaces, which can donate electrons to the Si NW,[28] showed minimal sensitivity response (hot plots). However, propynyl-modified sensor surfaces were the most reliable and stable when exposed to analytes. Therefore, propynyl-modified Si NWs had great selectivity toward identifying specific analytes. A combination of unmodified sensors (to identify analyte type/polarity), propenyl-modified sensors (for sensitivity and selectivity of nonpolar analytes), and propynyl-modified sensors (for increased stability and identification of analytes of similar molecular weights) always proved to be the most accurate sensor, where accuracies of over 79% of specific analyte detection were continuously achieved.

CONCLUSIONS

Molecular modifications were achieved and integrated into Si NW FETs. The sensing results showed that propenyl- and propynyl-modified sensors provided higher accuracy and sensitivity for specific analyte detection. Also, superior stabilities and sensitivities were achieved as surface coverage increased (i.e., trap states were reduced); however, the free electrons from the triple-bond present in the propynyl-modified sensors donated electrons to the Si NWs causing a saturation effect.

In addition, according to linear discriminant analysis models, propenyl- and propynyl-modified sensors (sensors S3−S6) proved to be more accurate in distinguishing specific analytes compared to unmodified sensors (sensor S1). Propyl-modified sensors (sensor S2) consistently performed with the least specificity because of the high noise levels, variability, and drift. Unmodified sensors consistently were able to selectively distinguish the type of analyte but not the specific analyte. However, the best accuracy was achieved by combining features from different sensors. In general, combining a feature from an unmodified sensor for the hydrophilic surface and a feature from a propenyl-modified sensor for increased sensitivity and stability afforded the highest analyte specificity.

ASSOCIATED CONTENT

Supporting Information

XPS of molecularly modified Si wafers, I_{ds} versus V_{gs} plots of sensors, and details of modified-Si NW FET sensor noise. The Supporting Information is available free of charge on the ACS Publications website at DOI: 10.1021/acsami.5b01721.

AUTHOR INFORMATION

Corresponding Author

*E-mail: hhossam@technion.ac.il.

Present Address

[†]The Dept. of Chemical Engineering, Univ. of New Hampshire, Durham, NH 03824, USA.

Author Contributions

The manuscript was written through contributions of all authors. All authors have given approval to the final version of the manuscript.

Notes

The authors declare no competing financial interest.

ACKNOWLEDGMENTS

The research leading to these results has received funding from the FP7-Health Program under the LCAOS (Grant Agreement No. 258868). J.M.H. acknowledges the Fulbright Foundation and Lady Davis Trust for financial support. The authors thank Ms. N. Shehadeh for fruitful discussions.

ABBREVIATIONS

FET = field effect transistor
Si = silicon
NW = nanowire

Symbols

F_a, flow of air through liquid analyte
F_T, flow of total air flow through system
I_{on}, on-current
I_{off}, off-current
S1, unmodified sensor
S2, propyl-modified sensor (55% coverage)
S3, propenyl-modified sensor (55% coverage)
S4, propenyl-modified sensor (100% coverage)
S5, propynyl-modified sensor (55% coverage)
S6, propynyl-modified sensor (100% coverage)
V_{th}, voltage threshold
μ_h, hole mobility
V_g, voltage between gate and source
V_{ds}, voltage between drain and source
I_{ds}, current between drain and source
$I_{V=x}$, current between drain and source at a specified voltage (x)
t_{ox}, thickness of oxide layer, 300 nm
n, number of nanowires on the FET, ∼50
R_{NW}, the radius of the Si NW, 40 nm
ε_{ox}, the dielectric constant of silicon oxide, 3.45×10^{-11}
L_{NW}, the length of the channel, 2 μm

REFERENCES

(1) Chen, X.; Wong, C. K. Y.; Yuan, C. A.; Zhang, G. Nanowire-Based Gas Sensors. *Sens. Actuators, B* **2013**, *177*, 178−195.

DOI: 10.1021/acsami.5b01721
ACS Appl. Mater. Interfaces 2015, 7, 11315−11321

(2) Feng, P.; Shao, F.; Shi, Y.; Wan, Q. Gas Sensors Based on Semiconducting Nanowire Field-Effect Transistors. *Sensors* **2014**, *14*, 17406−17429.
(3) Penner, R. M. Chemical Sensing with Nanowires. *Annu. Rev. Anal. Chem.* **2012**, *5*, 461−485.
(4) Engel, Y.; Elnathan, R.; Pevzner, A.; Davidi, G.; Flaxer, E.; Patolsky, F. Supersensitive Detection of Exlosives by Silicon Nanowire Arrays. *Angew. Chem., Int. Ed.* **2010**, *49*, 6830−6835.
(5) Ermanok, R.; Assad, O.; Zigelboim, K.; Wang, B.; Haick, H. Discriminative Power of Chemically Sensitive Silicon Nanowire Field Effect Transistors to Volatile Organic Compounds. *ACS Appl. Mater. Interfaces* **2013**, *5*, 11172−11183.
(6) Shehada, N.; Brönstrup, G.; Funka, K.; Christiansen, S.; Leja, M.; Haick, H. Ultrasensitive Silicon Nanowire for Real-World Gas Sensing: Noninvasive Diagnosis of Cancer from Breath Volatolome. *Nano Lett.* **2015**, *15*, 1288−1295.
(7) Wang, B.; Haick, H. Effect of Functional Groups on the Sensing Properties of Silicon Nanowires toward Volatile Compounds. *ACS Appl. Mater. Interfaces* **2013**, *5*, 2289−2299.
(8) Wang, B.; Haick, H. Effect of Chain Length on the Sensing of Volatile Organic Compounds by means of Silicon Nanowires. *ACS Appl. Mater. Interfaces* **2013**, *5*, 5748−5756.
(9) Paska, Y.; Stelzner, T.; Christiansen, S.; Haick, H. Enhanced Sensing of Nonpolar Volatile Organic Compounds by Silicon Nanowire Field Effect Transistors. *ACS Nano* **2011**, *5*, 5620−5626.
(10) Chang, Y.-M.; Kao, P.-H.; Tai, H.-M.; Wang, H.-W.; Lin, C.-M.; Lee, H.-Y.; Juang, J.-Y. Enhanced Field Emission Characteristics in Metal-Coated Si-Nanocones. *Phys. Chem. Chem. Phys.* **2013**, *15*, 10761−10766.
(11) de Smet, L. C. P. M.; Stork, G. A.; Hurenkamp, G. H. F.; Sun, Q.-Y.; Topal, H.; Vronen, P. J. E.; Sieval, A. B.; Wright, A.; Visser, G. M.; Zuilhof, H.; Sudholter, E. J. R. Covalently Attached Saccharides on Silicon Surfaces. *J. Am. Chem. Soc.* **2003**, *125*, 13916−13917.
(12) Gao, A.; Lu, N.; Dai, P.; Li, T.; Pei, H.; Gao, X.; Gong, Y.; Wang, Y.; Fan, C. Silicon-Nanowire-Based CMOS-Compatible Field-Effect Transistor Nanosensors for Ultrasensitive Electrical Detection of Nucleic Acids. *Nano Lett.* **2011**, *11*, 3974−3978.
(13) Jiao, J.; Nordlund, E.; Lindsey, J. S.; Bocian, D. F. Effects of Counterion Mobility, Surface Morphology, and Charge Screening on the Electron-Transfer Rates of Porphyrin Monolayers. *J. Phys. Chem. C* **2008**, *112*, 6173−6180.
(14) Pachauri, V.; Kern, K.; Balasubramanian, K. Field-Effect-Based Chemical Sensing Using Nanowire-Nanoparticle Hybrids: The Ion-Sensitive Metal-Semiconductor Field-Effect Transistors. *Appl. Phys. Lett.* **2013**, *102*, 023501−1−203501−5.
(15) Razgon, A.; Anstey, M. R.; Yakelis, N. A.; Bergman, R. G.; Sukenik, C. N. Surface Immobilization of an Organo-Iridium Complex through a Carbon-Metal Bond. *Inorg. Chim. Acta* **2011**, *375*, 305−307.
(16) Sun, Q.-Y.; de Smet, L. C. P. M.; van Lagen, B.; Wright, A.; Zuilhof, H.; Sudholter, E. J. R. Covalently Attached Monolayers on Hydrogen-Terminated Si(100): Extremely Mild Attachment by Visible Light. *Angew. Chem., Int. Ed.* **2004**, *43*, 1352−1355.
(17) Bashouti, M. Y.; Sardashti, K.; Schmitt, S. W.; Pietsch, M.; Ristein, J.; Haick, H.; Christiansen, S. H. Oxide-Free Hybrid Silicon Nanowires: From Fundamentals to Applied Nanotechnology. *Prog. Surf. Sci.* **2013**, *88*, 39−60.
(18) Bashouti, M. Y.; Stelzner, T.; Berger, A.; Christiansen, S.; Haick, H. Covalent Attachment of Alkyl Functionality to 50 nm Silicon Nanowires through a Chlorination/Alkylation Process. *J. Phys. Chem. C* **2009**, *113*, 14823−14828.
(19) Bashouti, M. Y.; Stelzner, T.; Berger, A.; Christiansen, S.; Haick, H. Chemical Passivation of Silicon Nanowires with C1−C6 Alkyl Chains through Covalent Si−C Bonds. *J. Phys. Chem. C* **2008**, *112*, 19168−19172.
(20) Bashouti, M. Y.; Paska, Y.; Puniredd, S. R.; Stelzner, T.; Christiansen, S.; Haick, H. Silicon Nanowires Terminated with Methyl Functionalities Exhibit Stronger Si-C Bonds than Equivalent 2D Surfaces. *Phys. Chem. Chem. Phys.* **2009**, *11*, 3845−3848.
(21) Wang, B.; Cancilla, J. C.; Torrecilla, J. S.; Haick, H. Artificial Sensing Intelligence with Silicon Nanowires for Ultraselective Detection in the Gas Phase. *Nano Lett.* **2014**, *14*, 933−938.
(22) Bashouti, M. Y.; Tung, R. T.; Haick, H. Tuning the Electrical Properties of Si Nanowires Field-Effect Transistors by Molecular Engineering. *Small* **2009**, *5*, 2761−2769.
(23) Haick, H.; Hurley, P. T.; Hochbaum, A. I.; Yang, P.; Lewis, N. S. Electrical Characteristics and Chemical Stability of Non-Oxidized, Methyl-Terminated Silicon Nanowires. *J. Am. Chem. Soc.* **2006**, *128*, 8990−8991.
(24) Paska, Y.; Haick, H. Interactive Effect of Hysteresis and Surface Chemistry on Gated Silicon Nanowire Gas Sensors. *ACS Appl. Mater. Interfaces* **2012**, *4*, 2604−2617.
(25) Paska, Y.; Stelzner, T.; Tisch, U.; Assad, O.; Christiansen, S.; Haick, H. Molecular Gating of Silicon Nanowire Field-Effect Transistors with Nonpolar Analytes. *ACS Nano* **2012**, *6*, 335−345.
(26) Bunimovich, Y. L.; Shin, Y. S.; Yeo, W.-S.; Amori, M.; Kwong, G.; Heath, J. R. Quantitative Real-Time Measurements of DNA Hybridization with Alkylated Nonoxidized Silicon Nanowires in Electrolyte Solution. *J. Am. Chem. Soc.* **2006**, *128* (50), 16323−16331.
(27) Assad, O.; Puniredd, S. R.; Stelzner, T.; Christiansen, S.; Haick, H. Stable Scaffolds for Reacting Si Nanowires with further Organic Functionalities while Preserving Si-C Passivation of Surface Sites. *J. Am. Chem. Soc.* **2008**, *130*, 17670−17671.
(28) Puniredd, S. R.; Assad, O.; Haick, H. Highly Stable Organic Monolayers for Reacting Silicon with Further Functionalities: The Effect of the C-C Bond nearest the Silicon Surface. *J. Am. Chem. Soc.* **2008**, *130*, 13727−13734.
(29) Soria, F. A.; Paredes-Olivera, P.; Patrito, E. M. Chemical Stability toward O_2 and H_2O of Si(111) Grafted with —CH_3, —$CH_2CH_2CH_3$, —$CHCHCH_3$, and —$CCCH_3$. *J. Phys. Chem. C* **2015**, *119* (1), 284−295.
(30) Puniredd, S. R.; Assad, O.; Haick, H. Highly Stable Organic Modification of Si(111) Surfaces: Towards Reacting Si with Further Functionalities while Preserving the Desirable Chemical Properties of Full Si−C Atop Site Terminations. *J. Am. Chem. Soc.* **2008**, *130*, 9184−9185.
(31) Puniredd, S. R.; Platzman, I.; Tung, R. T.; Haick, H. Bidirectional Control of Silicon's Surface Potential by Means of Molecular Coverage. *J. Phys. Chem. C* **2010**, *114* (43), 18674−18678.
(32) Ghosh-Mukerji, S.; Haick, H.; Paz, Y. Controlled mass transport as a means for obtaining selective photocatalysis. *J. Photochem. Photobiol., A* **2003**, *160*, 77−85.
(33) Stelzner, T.; Andra, G.; Wendler, E.; Wesch, W.; Scholz, R.; Gosele, U.; Christansen, S. Growth of Silicon Nanowires by Chemical Vapour Deposition on Gold Implanted Silicon Substrates. *Nanotechnology* **2006**, *17*, 2895−2898.
(34) Bansal, A.; Li, X.; Lauermann, I.; Lewis, N. S.; Yi, S. I.; Weinberg, W. H. Alkylation of Si Surfaces Using a Two-Step Halogenation/Grignard Route. *J. Am. Chem. Soc.* **1996**, *118*, 7225−7226.
(35) Wang, B.; Stelzner, T.; Dirawi, R.; Assad, O.; Shehada, N.; Christiansen, S.; Haick, H. Field-Effect Transistors Based on Silicon Nanowire Arrays: Effect of the Good and the Bad Silicon Nanowires. *ACS Appl. Mater. Interfaces* **2012**, *4*, 4251−4258.
(36) Assad, O.; Leshansky, A. M.; Wang, B.; Stelzner, T.; Christiansen, S.; Haick, H. Spray-Coating Route for Highly Aligned and Large-Scale Arrays of Nanowires. *ACS Nano* **2012**, *6*, 4702−4712.
(37) Haick, H.; Ambrico, M.; Ghabboun, J.; Ligonzo, T.; Cahen, D. Contacting Organic Molecules by Metal Evaporation. *Phys. Chem. Chem. Phys.* **2004**, *6*, 4538−4541.

DOI: 10.1021/acsami.5b01721
ACS Appl. Mater. Interfaces 2015, 7, 11315−11321